Nuclear Medicine and Biology 118-119 (2023) 108338

Contents lists available at ScienceDirect

Nuclear Medicine and Biology

journal homepage: www.elsevier.com/locate/nucmedbio

Direct comparison of [^{18}F]AlF-NOTA-JR11 and [^{18}F]AlF-NOTA-octreotide for PET imaging of neuroendocrine tumors: Antagonist *versus* agonist☆

Stephen Ahenkorah [a,b], Christopher Cawthorne [c], Erika Murce [d], Christophe M. Deroose [c,e], Thomas Cardinaels [a,f], Yann Seimbille [d], Guy Bormans [b], Maarten Ooms [a], Frederik Cleeren [b,*]

[a] NURA Research Group, Belgian Nuclear Research Center (SCK CEN), Mol, Belgium
[b] Radiopharmaceutical Research, Department of Pharmacy and Pharmacology, University of Leuven, Leuven, Belgium
[c] Nuclear Medicine and Molecular Imaging, Department of Imaging and Pathology, University of Leuven, Leuven, Belgium
[d] Department of Radiology and Nuclear Medicine, Erasmus MC, Rotterdam, the Netherlands
[e] Nuclear Medicine, University Hospitals Leuven, Campus Gasthuisberg, Leuven, Belgium
[f] Department of Chemistry, University of Leuven, Leuven, Belgium

ARTICLE INFO

Keywords:
Al^{18}F
NOTA-JR11
NOTA-octreotide
Somatostatin
Antagonist

ABSTRACT

Background: [^{18}F]AlF-NOTA-octreotide is an ^{18}F-labeled somatostatin analogue which is a good clinical alternative for ^{68}Ga-labeled somatostatin analogues. However, radiolabeled somatostatin receptor (SSTR) antagonists might outperform agonists regarding imaging sensitivity of neuroendocrine tumors (NETs). No direct comparison between the antagonist [^{18}F]AlF-NOTA-JR11 and the agonist [^{18}F]AlF-NOTA-octreotide as SSTR PET probes is available. Herein, we present the radiosynthesis of [^{18}F]AlF-NOTA-JR11 and compare its NETs imaging properties directly with the established agonist radioligand [^{18}F]AlF-NOTA-octreotide preclinically.
Methods: [^{18}F]AlF-NOTA-JR11 was synthesized in an automated synthesis module. The *in vitro* binding characteristics (IC_{50}) of [^{nat}F]AlF-NOTA-JR11 and [^{nat}F]AlF-NOTA-octreotide were evaluated and the *in vitro* stability of [^{18}F]AlF-NOTA-JR11 was determined in human serum. *In vitro* cell binding and internalization was performed with [^{18}F]AlF-NOTA-JR11 and [^{18}F]AlF-NOTA-octreotide using SSTR2 expressing cells and the pharmacokinetics were evaluated using μPET/CT in mice bearing BON1.SSTR2 tumor xenografts.
Results: Excellent binding affinity for SSTR2 was found for [^{nat}F]AlF-NOTA-octreotide (IC_{50} of 25.7 ± 7.9 nM). However, the IC_{50} value for [^{nat}F]AlF-NOTA-JR11 (290.6 ± 71 nM) was 11-fold higher compared to [^{nat}F]AlF-NOTA-octreotide, indicating lower affinity for SSTR2. [^{18}F]AlF-NOTA-JR11 was obtained in a good RCY (50 ± 6 %) but with moderate RCP of 94 ± 1 %. [^{18}F]AlF-NOTA-JR11 demonstrated excellent stability in human serum (>95 % after 240 min). 2.7-fold higher cell binding was observed for [^{18}F]AlF-NOTA-JR11 as compared to [^{18}F]AlF-NOTA-octreotide after 60 min. μPET/CT images demonstrated comparable pharmacokinetics and tumor uptake between [^{18}F]AlF-NOTA-JR11 (SUV_{max}: 3.7 ± 0.8) and [^{18}F]AlF-NOTA-octreotide (SUV_{max}: 3.6 ± 0.4).
Conclusions: [^{18}F]AlF-NOTA-JR11 was obtained in good RCY, albeit with a moderate RCP. The cell binding study showed significant higher binding of [^{18}F]AlF-NOTA-JR11 compared to [^{18}F]AlF-NOTA-octreotide, despite the higher IC_{50} value of AlF-NOTA-JR11. However, pharmacokinetics and *in vivo* tumor uptake was comparable for both radiotracers. Novel Al^{18}F-labeled derivatives of JR11 with higher SSTR2 affinity should be developed for increased tumor uptake and NET imaging sensitivity.

1. Introduction

Radiolabeled somatostatin receptor (SSTR) agonists, such as [^{68}Ga]Ga-DOTA-TATE and [^{177}Lu]Lu-DOTA-TATE, have become important tools for the diagnosis and treatment of patients with neuroendocrine tumors (NETs), respectively [1,2]. [^{18}F]AlF-NOTA-octreotide (Fig. 1), a promising ^{18}F-labeled somatostatin analogue (agonist) and potential alternative for ^{68}Ga-DOTA-peptides, is under clinical evaluation [3–5].

☆ This is a free access article and can be viewed on the journal's Web site (www.nucmedbio.com). Complimentary access to this article is available until the next issue publishes online.

* Corresponding author at: NURA Research Group, Belgian Nuclear Research Center (SCK CEN), Mol, Belgium.
E-mail address: frederik.cleeren@kuleuven.be (F. Cleeren).

https://doi.org/10.1016/j.nucmedbio.2023.108338
Received 19 January 2023; Received in revised form 14 March 2023; Accepted 27 March 2023
Available online 29 March 2023

The Al^{18}F-method combines the advantages of chelator based radiolabeling method with the logistical advantages of ^{18}F [6].

The longer half-life of ^{18}F compared to ^{68}Ga ($T_{1/2}$: 109.8 min *versus* 68 min respectively) enables imaging patients at later time points after injection, which may improve detection rates. Further, due to the high yield cyclotron production of ^{18}F, more patients can be injected with a single batch production and ^{18}F-labeled tracers can be produced centrally and transported to PET centres without onsite radiopharmaceutical production facilities.

SSTR agonists are known to undergo internalization of the ligand-receptor complex after high-affinity binding to the receptor, which was long seen as an ideal property of a vector molecule for PET applications [7]. However, Ginj et al. were the first to show in a preclinical setting that radiolabeled SSTR antagonists can outperform agonists for targeting NETs [8]. The current hypothesis for this observation is that antagonists bind to a greater number of binding sites than agonists [8].

A direct preclinical comparison revealed a two-fold higher tumor uptake of radiolabeled antagonist [^{111}In]In-DOTA-[p-NO_2-Phe-c(DCys-Tyr-DTrp-Lys-Thr-Cys) DTyr-NH_2] ([^{111}In]In-DOTA-BASS; IC_{50} = 9.4 ± 0.4 nM) *versus* agonist [^{111}In]In-diethylenetriaminepentaacetic acid (DTPA)-TATE using HEK293-SSTR2-tumor bearing mice [8]. Furthermore, *in vitro* receptor autoradiography revealed that [^{177}Lu]Lu-DOTA-BASS accumulated approximately four times more in SSTR2-expressing human tumor samples than the SSTR agonist [^{177}Lu]Lu-DOTA-TATE [9]. However, ^{64}Cu-labeled 4,11-bis(carboxymethyl)-1,4,8,11-tetraazabicyclo[6.6.2]hexadecane-BASS ([^{64}Cu]Cu-CB-TE2A-BASS) rather demonstrated lower tumor uptake compared to the agonist [^{64}Cu]Cu-CB-TE2A-Y3-TATE in rat pancreatic AR42J xenografts [10].

To overcome this limitation, the next generation of SSTR antagonists including JR10 ((*p*-NO_2-Phe-c[d-Cys-Tyr-d-Aph(Cbm)-Lys-Thr-Cys]-d-Tyr-NH_2; DOTA-JR10 IC_{50} = 0.62 ± 0.21 nM)) and JR11 ((Cpa-c[d-Cys-Aph(Hor)-d-Aph(Cbm)-Lys-Thr-Cys]-d-Tyr-NH_2; DOTA-JR11 IC_{50} = 0.72 ± 0.12 nM)) was developed to improve receptor affinity. Among these antagonists, radiolabeled JR11 derivatives such as [^{68}Ga]Ga-DOTA-JR11 for imaging applications and [^{177}Lu]Lu-DOTA-JR11 for therapy demonstrated the best affinity [11,12]. As a result, several (pre) clinical studies using JR11 as vector molecule have demonstrated its promising potentials as a targeting vector molecule for imaging and treatment of NETs [13–16]. For example, a first-in-human study of metastasized neuroendocrine neoplasias patients demonstrated higher tumor doses of [^{177}Lu]Lu-DOTA-JR11 (3.5-fold) *versus* [^{177}Lu]Lu-DOTA-TATE [17].

Hence, the SSTR2 antagonist JR11 might be an ideal vector molecule in combination with the Al^{18}F-method, offering improved imaging properties for NETs in combination with logistical advantages over ^{68}Ga-tracers such as [^{68}Ga]Ga-DOTA-JR11.

Xie et al. described the manual synthesis of [^{18}F]AlF-NOTA-JR11 (Fig. 1), cellular uptake, internalization, and saturation binding using HEK293-SSTR2 cells. Biodistribution and micro-PET imaging studies were carried out in HEK293-SSTR2 tumor-bearing mice and a pilot clinical PET/CT imaging study on ten patients with neuroendocrine neoplasms was performed with [^{18}F]AlF-NOTA-JR11 and compared with the clinical established tracer [^{68}Ga]Ga-DOTA-TATE [18]. The authors observed improved imaging properties of [^{18}F]AlF-NOTA-JR11 compared to [^{68}Ga]Ga-DOTA-TATE. However, no direct comparison between the antagonist [^{18}F]AlF-NOTA-JR11 and the agonist [^{18}F]AlF-NOTA-octreotide is available.

In this study, our aim was to automate the radiosynthesis of [^{18}F]AlF-NOTA-JR11 and to compare its NETs imaging properties directly with the established radioligand [^{18}F]AlF-NOTA-octreotide in a preclinical setting. We evaluated the *in vitro* binding characteristics (IC_{50}) of [^{nat}F]AlF-NOTA-JR11 and [^{nat}F]AlF-NOTA-octreotide and assessed the *in vitro* stability, *in vitro* cellular uptake and internalization of [^{18}F]AlF-NOTA-JR11 and [^{18}F]AlF-NOTA-octreotide using SSTR2-overexpressing cells. Further *in vivo* tumor accumulation of both tracers was compared using μPET/CT studies in QGP1-SSTR2 and BON1-SSTR2 tumor-bearing mice.

2. Experimental section

2.1. Materials

2.1.1. Reagents and solvents

All chemicals and solvents were purchased from commercial suppliers such as Sigma-Aldrich (Bornem, Belgium), Fluka (Bornem, Belgium), Fisher (Doornik, Belgium) and Acros Organics (Geel, Belgium) and were used without further purification. All radiolabeling buffers were treated with Chelex 100 [sodium form (50–100 mesh, Sigma Aldrich)] for 15 min to remove trace metals. All solutions were degassed and filtered before use.

2.2. Metal complex membrane-based affinity studies

2.2.1. Cold synthesis of [^{nat}F]AlF-NOTA-JR11 and [^{nat}F]AlF-NOTA-octreotide

The reaction was started by adding 490 μL $AlCl_3$ (5.1 mM in 0.1 M sodium acetate, pH 4.1, 10 equiv.) to 10 μL NaF (10 mg/mL in 0.1 M sodium acetate, pH 4.1, 10 equiv.) and the reaction mixture was stirred for 5 min. 500 μL of absolute ethanol was added to the aluminum fluoride mixture and added to 1 mg NOTA-JR11 trifluoroacetate (ABX, Radeberg, Germany) or NOTA-octreotide trifluoroacetate (ABX). The reaction was heated at 95 °C for 30 min. Water (V = 10 mL, high-performance capillary electrophoresis (HPCE) grade; Sigma-Aldrich) was used to dilute the reaction mixture after cooling for 10 min and this was loaded onto a Sep-Pak Plus Light C_{18} cartridge (Waters, Milford, Massachusetts) that was pretreated with 3 mL absolute EtOH and 3 mL water. Next, the cartridge was rinsed with 2 mL water and the purified ligand was eluted with 1 mL absolute ethanol into a vial. The ethanol was evaporated under vacuum and 1 mL of water and 0.5 mL of acetonitrile (LC-MS grade) was added. The mixture was sonicated for 5 min and filtered using a Captiva PTFE + GF 0.45 μm filter (Agilent,

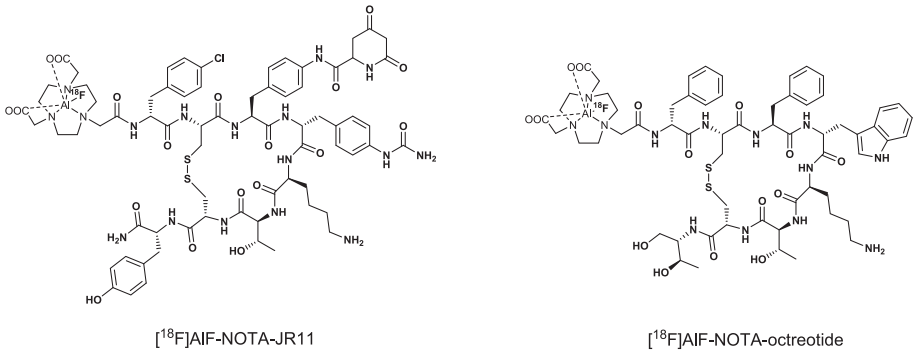

Fig. 1. Chemical structures of [^{18}F]AlF-NOTA-JR11 and [^{18}F]AlF-NOTA-octreotide.

Santa Clara, CA). The compounds were analyzed using HRMS by a Dionex Ultimate 3000 LC System (Dionex, Germering, Germany) coupled to a high-resolution time-of-flight mass spectrometer (maXis impact, Bruker, Bremen, Germany) equipped with an orthogonal electrospray ionization interface (UPLC-HRMS). Acquisition and processing of data were performed using HyStar® and Compass DataAnalysis® (version 4.1, Bruker) respectively. Table 1 provides mass data and purity of the cold compounds.

Competition binding studies (IC_{50}) were performed as previously described using purified Chinese hamster ovary-K1 (CHO-K1) cell membranes overexpressing human SSTR2 (Perkin Elmer, Zaventem, Belgium) [19]. Briefly, prior to the assay, the plate filters were pre-soaked in 200 μL 0.1 % polyethylenimine for 1 h at room temperature (rt). The assay buffer consists out of 25 mM HEPES pH 7.4, 10 mM $MgCl_2$, 1 mM $CaCl_2$ and 0.5 % Bovine Serum Albumin (BSA), while the washing buffer consisted out of 50 mM Tris-HCl pH 7.4, 0.2 % BSA. Human $SSTR2^+$ membranes derived from CHO-K1 cells (1 × 400 units, 25 μg protein/unit) were prepared as follows: 0.125 mL of membrane + 4.875 mL assay buffer (1:40 dilution). Following pre-incubation, the diluted membranes (178 μL), [^{111}In]In-DOTA-TATE (2 μL, 10^{-9} M), and various concentrations of the competing non-radioactive compounds [^{nat}F]AlF-NOTA-JR11 or [^{nat}F]AlF-NOTA-octreotide (20 μL, 10^{-12}–10^{-5} M) were added to each well, for a total volume of 200 μL/well. The plates were incubated at rt for 90 min. After incubation, the solution in each well was filtered using a vacuum manifold and followed by ten washes with ice-cold wash buffer (200 μL, each wash was filtered through). Each plate filter was removed carefully, placed in a counting tube and activity was measured in the gamma counter. The assay measures binding affinity (IC_{50}) by evaluating the ability of the compounds [^{nat}F]AlF-NOTA-JR11 and [^{nat}F]AlF-NOTA-octreotide to compete with the radioactive reference ligand [^{111}In]In-DOTA-TATE for SSTR2 binding sites on CHO-K1 membranes. IC_{50} values were calculated using nonlinear regression (four parameters) using GraphPad Prism 9 (Graph Pad Software, San Diego, CA, USA) based on three independent biological replicates for each concentration tested.

2.3. Radiochemistry

2.3.1. Radio-synthesis and QC system

[^{18}F]AlF-NOTA-JR11 was synthesized in an automated AllinOne® synthesis module (Trasis, Ans, Belgium) as follows: during the placement of vials and reagents on the cassette, 25 μL of 2 mM aluminum chloride ($AlCl_3$, anhydrous, powder, 99.999 % trace metals basis, Sigma-Aldrich) in sodium acetate buffer (0.1 M, pH 4.1) was added to the 4 mL cyclic olefin copolymer reactor.

[^{18}F]fluoride (9.8 ± 2.4 GBq) was transferred to the module and trapped on a Sep-Pak light Accel plus anion exchange cartridge (Cl^- form: Waters). Subsequently, the cartridge was washed with 6 mL of water (HPCE grade, Sigma Aldrich). [^{18}F]fluoride was eluted from the QMA cartridge into a reservoir (5 mL Inject syringe; BBraun, Melsungen, Germany) with 500 μL of the eluent solution, containing 250 μL NaCl 0.9 % ((99.999 % trace metals basis NaCl (Sigma Aldrich) in HPCE grade water (Sigma Aldrich)) and 250 μL absolute ethanol. 250 μL of the [^{18}F]fluoride containing eluate was transferred to the reactor containing the $AlCl_3$ solution. To form [^{18}F]AlF, the solution was stirred for 2 min at rt. under gentle nitrogen flow (N_2).

Table 1
Mass data and purity of [^{nat}F]AlF-NOTA-JR11 and [^{nat}F]AlF-NOTA-octreotide.

Compound	Expected mass	Observed mass	Purity (LC 220 nm)
[^{nat}F]AlF-NOTA-JR11	1632.7854 Da	1632.7837 ± 0.02 Da	>96
[^{nat}F]AlF-NOTA-octreotide	1348.7545 Da	1348.7547 ± 0.02 Da	>96

The precursor solution (600 μL of 0.2 mg/mL NOTA-JR11 trifluoroacetate) and 0.95 mg/mL sodium ascorbate in sodium acetate 0.1 M pH 4.1/absolute ethanol (50/50 V/V) was added to the reactor, which was then sealed and heated for 10 min at 100 °C. After transfer to the reactor, approximately 100 μL of precursor solution remained in the precursor vial. After cooling the reactor to 40 °C, the reaction mixture was transferred to a dilution vial filled with 15 mL formulation solution (0.59 % NaAsc in 0.9 % NaCl solution) and mixed under gentle nitrogen flow (N_2). The diluted solution was applied to a Sep-Pak light C_{18} cartridge (Waters) that had been preconditioned with 3 mL absolute EtOH and 3 mL water. Following that, the cartridge was washed with 20 mL formulation solution and flushed with nitrogen to remove unreacted [^{18}F]AlF and free [^{18}F]fluoride. [^{18}F]AlF-NOTA-JR11 was eluted with 1.8 mL absolute ethanol from the SPE cartridge to the dispensing cell, and the SPE cartridge was flushed with 17.2 mL of the formulation solution.

The eluate was passed through a 0.22 μm sterile filter (Millex-GV, 0.22 μm, PVDF, 13 mm, Merck KGaA, Darmstadt, Germany) into a sterile 25 mL dose vial. The final drug product solution ([^{18}F]AlF-NOTA-JR11 in ((0.59 % NaAsc in 0.9 % NaCl solution)) was measured in an ionization chamber-based dose calibrator (COMECER VIK-203, Comecer S.p.A., Castel Bolognese, Italy) and samples were taken for quality control. [^{18}F]AlF-NOTA-octreotide was synthesized as previously described [13]. High pressure liquid chromatography (a Shimadzu LC20A HPLC System, Shimadzu, Kyoto, Japan) coupled in series to a DAD-UV detector (wavelength = 220 nm) and a shielded 3-in. NaI (Tl) scintillation detector connected to a single channel analyzer (Gabi box, Elysia-Raytest, Straubenhardt, Germany) was used for the identification and the determination of radiochemical purity (RCP) of [^{18}F]AlF-NOTA-JR11. Recovery of [^{18}F]AlF and [^{18}F]F^- on this system is >95 %, as earlier determined by Tshibangu et al. [20,21]. HPLC column: C_{18} column (Waters XBridge® 3.5 μm, 3.0 × 100 mm); mobile phase composition: A (0.05 M ammonium acetate, pH = 5.5): 0–5 min (95 %), 5–25 min (80 → 75 %), 25.1–30 min (95 %); B (acetonitrile): 0–5 min (5 %), 5–25 min (20 → 25 %), 25.1–30 min (5 %); flowrate of 0.8 mL/min.

2.3.2. In vitro stability of [^{18}F]AlF-NOTA-JR11

50 μL of purified [^{18}F]AlF-NOTA-JR11 (5–10 MBq) was added to a 1 mL vial containing either 450 μL of PBS, human serum or formulation buffer and the solution was incubated at 37 °C under constant gentle shaking (Eppendorf ThermoMixer®, Hamburg, Germany). To determine the percentage (%) of intact [^{18}F]AlF-NOTA-JR11, 5 μL of the reaction mixture was taken for analysis at 10, 30, 60, 120 and 240 min whiles radio-HPLC was determined at 240 min. The fraction of intact tracer was evaluated by radio-HPLC (see method above). Stability of [^{18}F]AlF-NOTA-octreotide was already reported using the same method [20].

2.3.3. Cell binding and internalization

Cellular uptake and internalization of [^{18}F]AlF-NOTA-JR11 and [^{18}F]AlF-NOTA-octreotide on SSTR2 transfected BON1.SSTR2 and QGP1.SSTR2 cells were investigated [22]. Non-specific uptake was determined in the presence of 100 μM octreotide acetate at 60 min timepoint (ABX, Radeberg, Germany). Briefly, BON1.SSTR2 (4 × 10^5 cells) or QGP1.SSTR2 (3 × 10^5 cells) cells were cultured in a 24-well plate overnight. Adherent cells were incubated with the radioligand of interest (n = 3, 180–190 kBq/well) for 5, 10, 30, 60, 120, 180 and 240 min at 37 °C in the presence or absence of octreotide acetate (100 μM, n = 3). After incubation, the supernatant was removed, and the cells were washed with three times 250 μL/well ice-cold PBS and were added to the supernatant. Subsequently, cells were incubated twice with 50 mM glycine-HCl pH 2.8 (500 μL/well) for 5 min at rt. followed by three washing steps with ice-cold PBS (250 μL/well). Then, cells were lysed using 250 μL of reagent A100 (Chemometec, Allerod, Denmark). Reagent B (Chemometec) was used for rinsing the wells and to quench the lysing of the cells. Quantification of the amount of bound and internalized activity was performed using a gamma counter (Wallac Wizard

1480, PerkinElmer, Waltham, MA). The number of cells per well was counted using an automated counting device (NucleoCounter® NC-100™, Chemometec, Allerod, Denmark). Results were expressed as percentage of applied radioactivity bound to 10^6 cells.

2.3.4. Animals

Animals were kept in individually ventilated cages in a temperature-controlled (approximately 22 °C) and humidity-controlled facility with a 12 h–12 h light-dark cycle and unlimited access to food and water. All animal procedures were approved by the KU Leuven ethical review board (ethical approval reference P054/2021) and were carried out in accordance with Directive 2010/63/EU and reported according to the ARRIVE guidelines [22].

2.3.5. Preparation of tumor xenograft model

The subcutaneous tumor xenograft model was prepared following a published procedure [23]. Briefly, BON1.SSTR2 (5×10^6) or QGP1.SSTR2 (2×10^6) cells mixed with Cultrex (1:1; Cultrex Basement Membrane Extract, R&D systems, Minneapolis) and were implanted subcutaneously into the right shoulder of female 6–8 week-old SCID mice (SCID Beige C B17.Cg-Prkdc scid Lystbg-J/Crl; Charles River Laboratories, Sulzfeld, Germany). After an average of four weeks, the tumor mice were used in biodistribution and PET/computed tomography (CT) imaging studies. Tumor volumes ranged from 150 to 400 mm^3 (measured by caliper, h × l × w), while the tumor mass-to-body weight ratio was 0.16–2.44 %. All animals included in the study were randomly selected among the in-house bred mice of the correct age. There were no exclusion criteria, and all subsequent studies and analyses were conducted unblinded.

2.3.6. PET/CT imaging and biodistribution study

Small animal whole-body PET imaging was performed by intravenously administering [^{18}F]AlF-NOTA-JR11 or [^{18}F]AlF-NOTA-octreotide (1.5–3.0 MBq/mouse) in the presence or absence of octreotide acetate (5 mg/kg) into BON1.SSTR2 or QGP1.SSTR2 tumor-bearing mice. Dynamic PET images were acquired for 75 min immediately after intravenous injection using a β-cube PET scanner (Molecubes, Gent, Belgium). The mice were kept under gas anesthesia during the entire procedure (2.5 % isoflurane in O_2 at 1 L/min flow rate), with temperature and respiration monitored throughout. After PET scanning, a CT image was acquired for anatomic coregistration with an X-cube CT scanner (Molecubes), using the 'general' protocol with the following parameters: 50 kVp, 480 exposures, 85 ms/projection, 100 μA tube current, rotation time 60 s.

2.3.7. Image processing and analysis

PET data were histogrammed into 14 frames (4 × 15 s, 4 × 1 min, 1 × 5 min, 5 × 10 min) and reconstructed into a 192 × 192 image matrix with 0.4 mm voxels using 30 iterations the native MLEM algorithm with corrections for randoms, scatter, attenuation and decay. CT Data were reconstructed using a regularized statistical (iterative) image reconstruction algorithm using non-negative least squares, using an isotropic 200 μm voxel size and scaled to Hounsfield Units (HUs) after calibration against a standard air/water phantom. Using PFUS v4.0 to display the fused PET-CT image (PMOD Technologies GmbH, Zürich, Switzerland), volumes of interest were manually drawn over the tumor while a sphere of 3 mm diameter was placed over the left lobe of the liver.

2.3.8. Statistical analysis

Quantitative data are expressed as mean ± standard deviation (SD) unless stated otherwise. Means were compared using the independent-samples *t*-test (*t*-test: two-sample assuming unequal variances in Microsoft Excel). Values were considered statistically significant for $p < 0.05$.

3. Results and discussion

3.1. Metal complex membrane-based affinity studies

We assessed the *in vitro* binding characteristics (IC_{50}) of [^{nat}F]AlF-NOTA-JR11 and [^{nat}F]AlF-NOTA-octreotide on SSTR2-overexpressing CHO-K1 cell membranes using [^{111}In]In-DOTA-TATE as the competing ligand [5]. SSTR2 overexpressing cells were used in this assay because SSTR2 is the most abundant SSTR in the majority of NETs, even when other subtypes are present [7]. The IC_{50} value of DOTA-TATE was also determined for comparison (Table 2).

Excellent binding for SSTR2 was found for [^{nat}F]AlF-NOTA-octreotide (IC_{50} of 25.7 ± 7.9 nM). However, the IC_{50} value for [^{nat}F]AlF-NOTA-JR11 (290.6 ± 71.5 nM) was 11-fold higher compared to [^{nat}F]AlF-NOTA-Octreotide, indicating lower affinity for SSTR2. Xie et al. also reported a slightly higher K_d value for [^{18}F]AlF-NOTA-JR11 (Kd = 11.59 ± 1.02 nM) compared to [^{68}Ga]Ga-DOTA-TATE (K_d = 7.36 ± 1.31 nM), indicating indeed a lower affinity of [^{18}F]AlF-NOTA-JR11 compared to [^{68}Ga]Ga-DOTA-TATE for SSTR2. However, in this study HEK293-SSTR2 cells were used instead of SSTR2-overexpressing CHO-K1 cell membranes [18]. It might be of interest to determine the Kd of [^{18}F]AlF-NOTA-JR11 using BON1.SSTR2 or QGP.SSTR2 cells.

The IC_{50} observed for [^{nat}F]AlF-NOTA-octreotide was around 7-fold higher than what is reported in literature (3.6 ± 0.6 nM) [5], but this experiment was performed using the rat pancreatic AR42J cell line which expresses all SSTR subtypes. DOTA-TATE as such, on the other hand, exhibited the lowest IC_{50} value (4.6 ± 2.1 nM) in our experiment. According to Reubi et al., these noticeable changes in receptor affinity profiles are caused not only by the different charges, but also by the different chemical structures and hydrophilicity of these compounds [24]. Fani et al. has also shown that SSTR2 antagonists are particularly sensitive to N-terminal modifications which could lead to the higher IC_{50} value which was observed for [^{18}F]AlF-NOTA-JR11 [12].

3.2. Radiolabeling and in vitro stability of [^{18}F]AlF-NOTA-JR11

NOTA-JR11 was radiolabeled with [^{18}F]AlF in an automated AllinOne® synthesis module ([^{18}F]AlF-NOTA-octreotide method) [20] and the corresponding [^{18}F]AlF-NOTA-JR11 was obtained in good radiochemical yield (RCY) [(49.7 ± 6 %, (decay-corrected, activity final batch of purified product/activity in reactor, n = 6, apparent molar activity 27 ± 6 GBq/μmol)] but with an unsatisfactory radiochemical purity (RCP) of 91.8 ± 6 % (Fig. 2A).

[^{18}F]AlF-NOTA-JR11 eluted as two diastereomers at 12 and 13 min (peaks 1 and 2, respectively). Formation of two stereoisomers of [^{18}F]AlF-NOTA-JR11 is already reported in literature, and this was also reported for the agonist [^{18}F]AlF-NOTA-octreotide [5,18,20]. One hypothesis for this phenomena is that the metal chelation results in conformational difference depending on which side the metal binds to the macrocycle of the bi-functional chelator [25]. The fast conformational modification through continuous cycles of metal release and recombination leads to molecules with different physico-chemical properties such as hydrophilicity.

Radio-HPLC analysis (Fig. 2A) showed a relatively high fraction (~6 %) of free [^{18}F]F^- or [^{18}F]AlF species (retention time 1.5 min). Further, we also observed an unidentified radioactive impurity (~3 %) eluting

Table 2
IC_{50} values of the reference compounds using SSTR2 overexpressing CHO-K1 cell membranes (±SD, n = 3 (independent biological assays)).

Compound	IC_{50} (nM)
[^{nat}F]AlF-NOTA-JR11	290.6 ± 71.5
[^{nat}F]AlF-NOTA-octreotide	25.7 ± 7.9
DOTA-TATE	4.6 ± 2.1

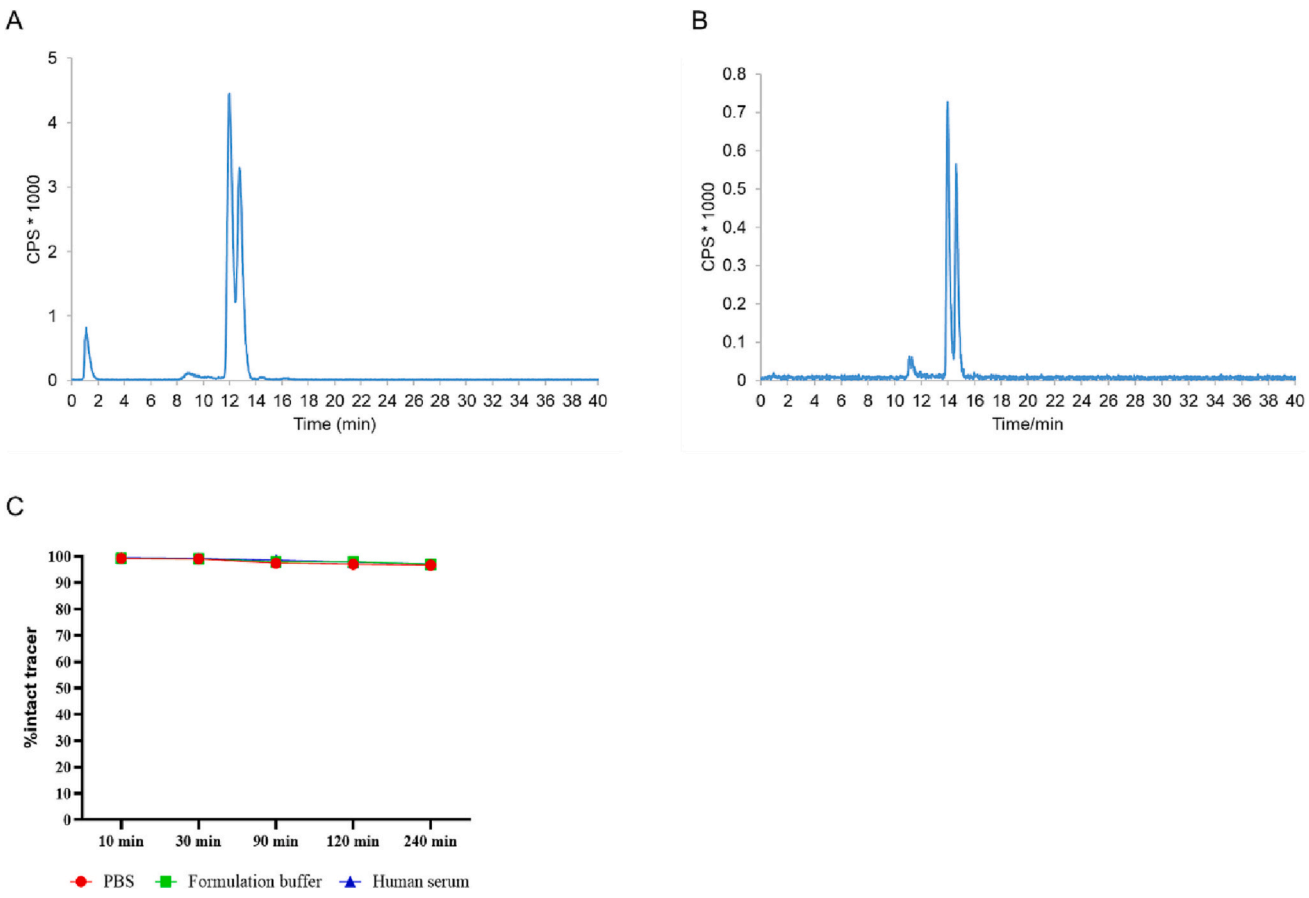

Fig. 2. HPLC radiochromatogram of (A) [^{18}F]AlF-NOTA-JR11 after automated radiosynthesis and purification. A RCP of 91.8 % ([^{18}F]AlF-NOTA-JR11, retention: 12 and 13 min for peaks 1 and 2 respectively) was observed with ~6 % free [^{18}F]F^- or [^{18}F]AlF (retention: 1.5 min) and extra radioactive impurity eluting before [^{18}F]AlF-NOTA-JR11; (B) [^{18}F]AlF-NOTA-JR11 after automated radiosynthesis and purification with altered synthetic sequence. A RCP of 94 % ([^{18}F]AlF-NOTA-JR11, retention: 14 and 15 min for peak 1 and 2 respectively) was observed with <1 % free [^{18}F]F^- or [^{18}F]AlF (retention: 1.5 min) and an extra radioactive impurity (~6 %) eluting before [^{18}F]AlF-NOTA-JR11. (C) *In vitro* stability of [^{18}F]AlF-NOTA-JR11. The stability of [^{18}F]AlF-NOTA-JR11 was evaluated in PBS, formulation buffer and human serum at 37 °C up to 4 h after end of synthesis.

before [^{18}F]AlF-NOTA-JR11.

To improve the RCP, we modified the radiosynthesis parameters by changing the synthesis sequence on the AllinOne® synthesis module. As we suspected that traces of unbound [^{18}F]F^- or [^{18}F]AlF-species were still present in the tubing where our final elution step with absolute ethanol took place, we bypassed this tubing and as a result we did not observe free [^{18}F]F^- or [^{18}F]AlF-species. Radio-HPLC analysis (Fig. 2B) showed <1 % of unbound [^{18}F]F or [^{18}F]AlF species. However, the unidentified impurity was still present in the radiochromatogram resulting in a RCP of 94 %.

As [^{18}F]AlF-NOTA-JR11 showed higher lipophilicity on the HPLC system compared to the unwanted impurity, we tried to purify the radiocomplex *via* solid phase extraction (Sepak Plus light, C_{18}, Waters) by varying the concentration of absolute ethanol of the washing solution (5 %–40 %), but were unsuccessful as it was not possible to isolate [^{18}F]AlF-NOTA-JR11 from the impurity. Similar results were observed by Xie et al. and they isolated [^{18}F]AlF-NOTA-JR11 with semi-preparative reversed-phase HPLC to obtain a final RCP of 98.74 ± 1.24 % [20].

As published by Tshibangu et al., a RCP of ≥91 % [^{18}F]AlF-NOTA-octreotide of total radioactivity, with ≤5 % sum of [^{18}F]F^- and [^{18}F]AlF, as determined with radio-HPLC, was required as acceptance criteria [20]. However, in the monograph 07/2021:3116 "PSMA-1007 (^{18}F) injection", a radiochemical purity of ≥95 % [^{18}F]F-PSMA-1007 of total radioactivity, with ≤5 % sum of [^{18}F]F^- and [^{18}F]AlF, as determined with radio-HPLC, is advised as acceptance criteria. Therefore, for possible future clinical translation, semi-preparative reversed-phase HPLC purification is recommended to increase the RCP above 95 %. Radio-HPLC analysis of [^{18}F]AlF-NOTA showed an excellent *in vitro* stability with >95 % intact complex of the starting radiotracer up to 4 h in all tested conditions (human serum, PBS and formulation buffer, Fig. 2C).

3.3. Cell binding and internalization

Membrane binding and internalization of [^{18}F]AlF-NOTA-JR11 and [^{18}F]AlF-NOTA-octreotide on BON1.SSTR2 and QGP1.SSTR2 cells were investigated in the absence or presence of excess octreotide acetate (100 μM). BON1 and QGP1 are originally of human origin derived pancreatic NETs and are transfected with pcDNA3.1-huSSTR2 to overexpress the human SSTR2 [22]. We employed these recombinant cell lines to evaluate the cell binding profile of [^{18}F]AlF-NOTA-JR11 and [^{18}F]AlF-NOTA-octreotide towards SSTR2. The total cell-bound fraction of [^{18}F]AlF-NOTA-JR11 on both cell lines was observed to be higher than that of [^{18}F]AlF-NOTA-octreotide, which is counterintuitive because the observed IC_{50} value of [^{18}F]AlF-NOTA-JR11 was 11-fold higher than for [^{18}F]AlF-NOTA-octreotide. After 60 min incubation, 75.9 ± 0.8 % binding (of which 4.5 ± 0.5 was internalized) as compared to 28.1 ± 1.9 % binding (of which 21.2 ± 1.7 % was internalized) were recorded for [^{18}F]AlF-NOTA-JR11 and [^{18}F]AlF-NOTA-octreotide respectively using BON1.SSTR2 cells (Fig. 3A).

Similar results were observed when using the QGP1.SSTR2 cell line. After 60 min incubation, 85.2 ± 0.9 % binding of [^{18}F]AlF-NOTA-JR11

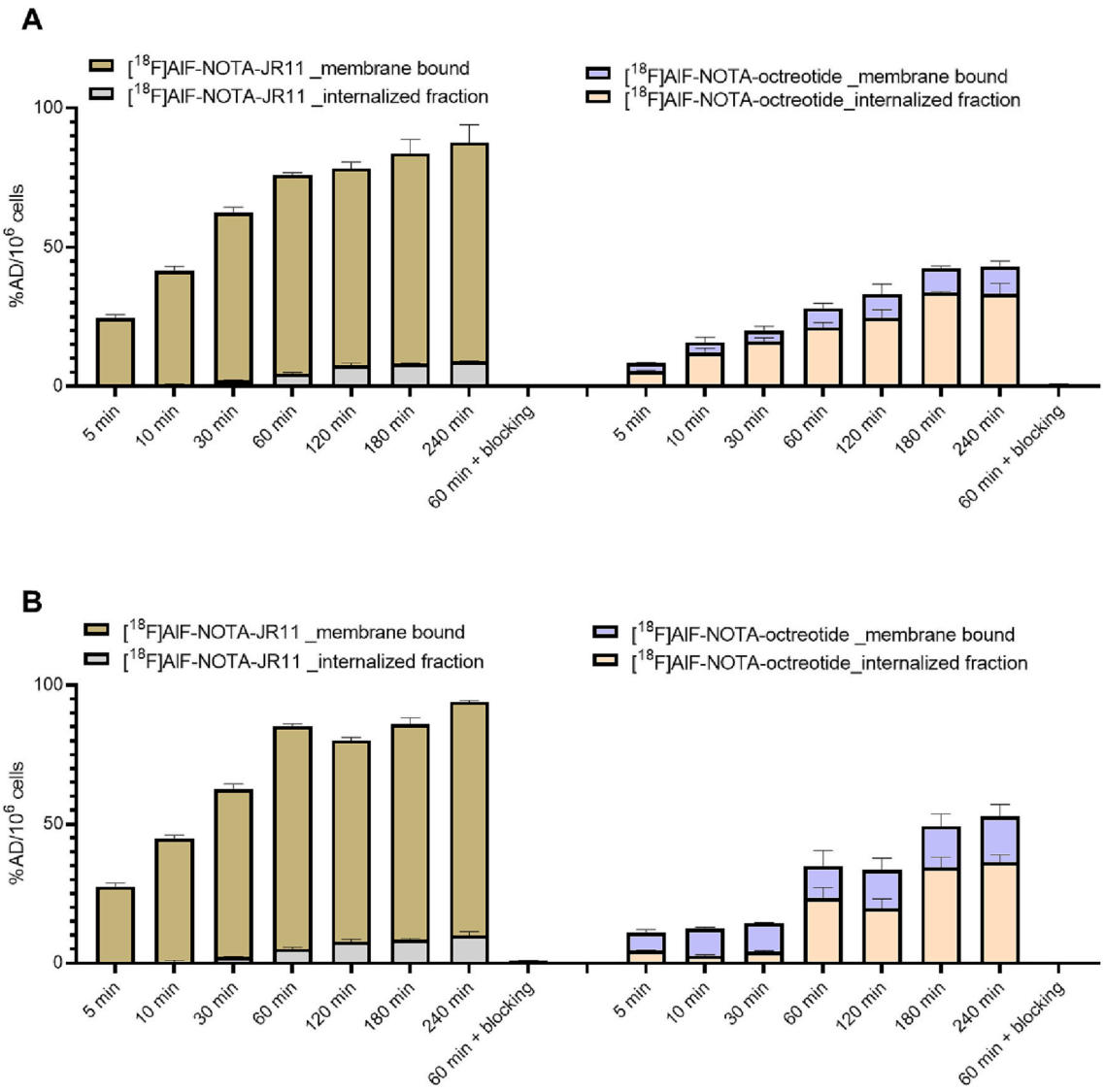

Fig. 3. Cell binding and internalization of [^{18}F]AlF-NOTA-octreotide and [^{18}F]AlF-NOTA-JR11 on (A) BON1.SSTR2 and (B) QGP1.SSTR2 cell lines. Adherent cells were incubated with the radioligand of interest ($n = 3$, 180–190 kBq/well) for 5, 10, 30, 60, 120, 180 and 240 min at 37 °C in the presence or absence of octreotide acetate (100 μM, $n = 3$). AD = absorbed dose.

(of which 5.1 ± 0.6 % was internalized) was observed as compared to 34.9 ± 5.6 % binding of [^{18}F]AlF-NOTA-octreotide (of which 23.5 ± 3.6 was internalized). At 240 min, the total uptake of [^{18}F]AlF-NOTA-JR11 was approximately two times higher of that of [^{18}F]AlF-NOTA-octreotide for both cell lines (Fig. 3B). Furthermore, most radioactivity uptake of [^{18}F]AlF-NOTA-octreotide was internalized (>70 %), whereas only 10 % of the total bound fraction of [^{18}F]AlF-NOTA-JR11 was internalized after 240 min, consistent with the radiotracer receptor agonist *versus* receptor antagonist properties [8,26]. Little to no uptake was seen (>99 % blocking), when cells were incubated with 100 μM octreotide acetate for 60 min, demonstrating receptor specificity of both radiotracers (Fig. 3).

Dalm et al. observed up to five times more cellular uptake of [^{177}Lu]Lu-DOTA-JR11 compared to [^{177}Lu]Lu-DOTA-TATE using a human osteosarcoma SSTR2 transfected cell line (U2OS-SSTR2) after 4 h incubation. According to the authors, 12 % of the total bound fraction of [^{177}Lu]Lu-DOTA-JR11 was internalized whereas 74 % of [^{177}Lu]Lu-DOTA-TATE out of the total bound fraction was internalized [26]. This overall higher cellular uptake of the antagonist compared to the agonist analogue has been consistently observed and has been discussed in the literature by several groups [26,27]. However, there are only hypotheses about the cause of this difference in *in vitro* cellular uptake behavior by agonist and antagonist somatostatin analogues. The difference is explained by two types of receptor states: those that are coupled to G-proteins and those that are uncoupled [27]. Antagonists bind to all receptor states, whereas agonists only bind to G-protein-coupled forms, which are thought to represent a small proportion of the total receptor population. G-protein coupled receptors are frequently overexpressed in cancer, and the antagonist [^{125}I]I-JR11 has shown superior binding than the agonist [^{125}I]I-Tyr^3-octreotide towards the gastrin-releasing peptide receptor, SSTR2 and SSTR3, and the glucose-dependent insulinotropic polypeptide receptor (GIPR) [27,28].

On the contrary, Xie et al. observed surprisingly higher cellular uptake for [^{68}Ga]Ga-DOTA-TATE than for [^{18}F]AlF-NOTA-JR11 after 2 h incubation (8.90 ± 0.50 % AD *versus* 4.5 ± 0.3 % AD; AD is absorbed dose) using the HEK293-SSTR2 cell line [18]. These findings pave the way for further research into the *in vitro* affinity behavior of agonist and antagonist somatostatin analogues in relation to the conjugated chelator and radionuclide selection. We can speculate that the binding degree of these SSTR analogues is dependent on both the used cell line, vector molecule, chelator and radionuclide.

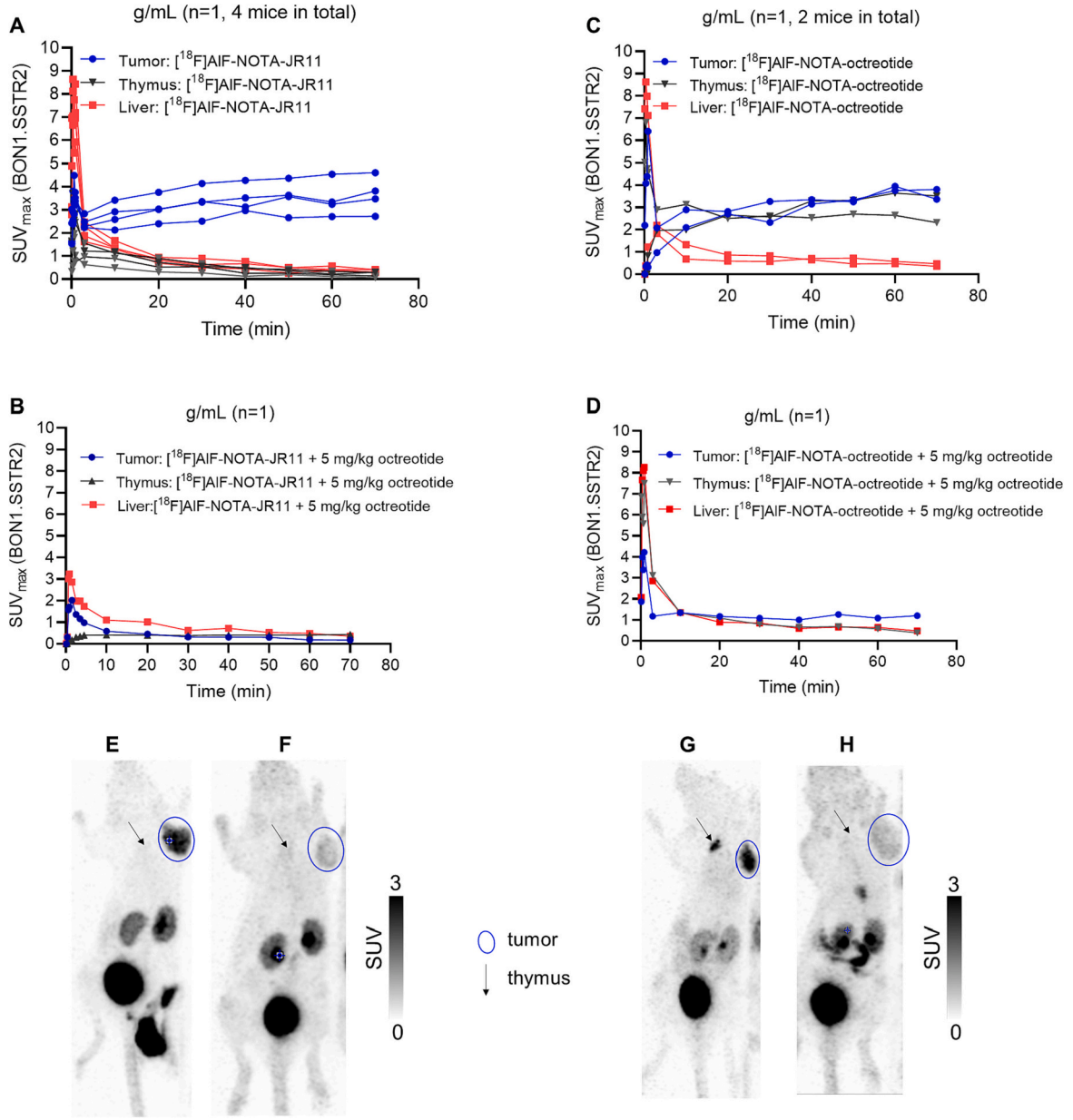

Fig. 4. TACs (SUV_{max}) representing PET/CT imaging of BON1.SSTR2 tumor-bearing mice: (A) [^{18}F]AlF-NOTA-JR11; (B) [^{18}F]AlF-NOTA-JR11 + 5 mg/kg octreotide; (C) [^{18}F]AlF-NOTA-octreotide; (D) [^{18}F]AlF-NOTA-octreotide + 5 mg/kg octreotide; MIP image (65–75 min p.i.): (E) [^{18}F]AlF-NOTA-JR11; (F) [^{18}F]AlF-NOTA-JR11 + 5 mg/kg octreotide; G) [^{18}F]AlF-NOTA-octreotide; (H) [^{18}F]AlF-NOTA-octreotide + 5 mg/kg octreotide. Blue circles and black arrows represent tumor and thymus regions respectively. (For interpretation of the references to color in this figure legend, the reader is referred to the web version of this article.)

3.4. In vivo imaging of [^{18}F]AlF-NOTA-JR11 and [^{18}F]AlF-NOTA-octreotide

μPET/CT images demonstrated fast clearance from the liver (SUV_{max} < 0.4) for both [^{18}F]AlF-NOTA-JR11 and [^{18}F]AlF-NOTA-octreotide (Figs. 4 & 5). [^{18}F]AlF-NOTA-JR11 showed fast clearance from the thymus (SUV_{max} < 0.2) in BON1.SSTR2 and QGP1.SSTR2 tumor bearing mice. However, [^{18}F]AlF-NOTA-octreotide demonstrated consistent and sustained uptake in the thymus (SUV_{max} > 2). The lower [^{18}F]AlF-NOTA-JR11 uptake in the thymus could be explained by the difference in SSTR affinities for [^{18}F]AlF-NOTA-JR11 and [^{18}F]AlF-NOTA-octreotide. Ten Bokum et al. has reported tissue distribution of octreotide binding receptors in normal mice and mice prone to autoimmunity. In this study, the authors observed high specific uptake of activity in the thymus (1–1.7 %ID/g) for all mice strains [29]. It was therefore not surprising to see uptake of [^{18}F]AlF-NOTA-octreotide in this organ in our study. Autoradiography with [^{125}I]I-octreotide in the human thymus revealed the existence of somatostatin receptor subtypes in the thymic medulla. However, [^{111}In]In-DTPA-octreotide was not taken up by the typical human thymus. SSTRs are expressed selectively in the thymus of various species, including humans, in both microenvironmental and lymphoid cells [29]. Their role, however, has to be investigated further.

Comparable tumor uptake between [^{18}F]AlF-NOTA-JR11 (SUV_{max}: 3.7 ± 0.8) and [^{18}F]AlF-NOTA-octreotide (SUV_{max}: 3.6 ± 0.4) was observed for the BON1.SSTR2 tumor bearing mice ($p = 0.96$). Also the tumor uptake of [^{18}F]AlF-NOTA-JR11 (SUV_{max}: 7.3 ± 2.4) for QGP1.SSTR2 tumor bearing mice was not significantly different to that of [^{18}F]AlF-NOTA-octreotide (SUV_{max}: 7.5 ± 1.9). Radiotracer uptake was reduced upon co-injection of 2.5 mg/kg octreotide acetate in line with previous reports, indicating SSTR2 specific uptake of both tracers as expected (Figs. 4 and 5).

Currently, there are contradictory reports regarding the tumor

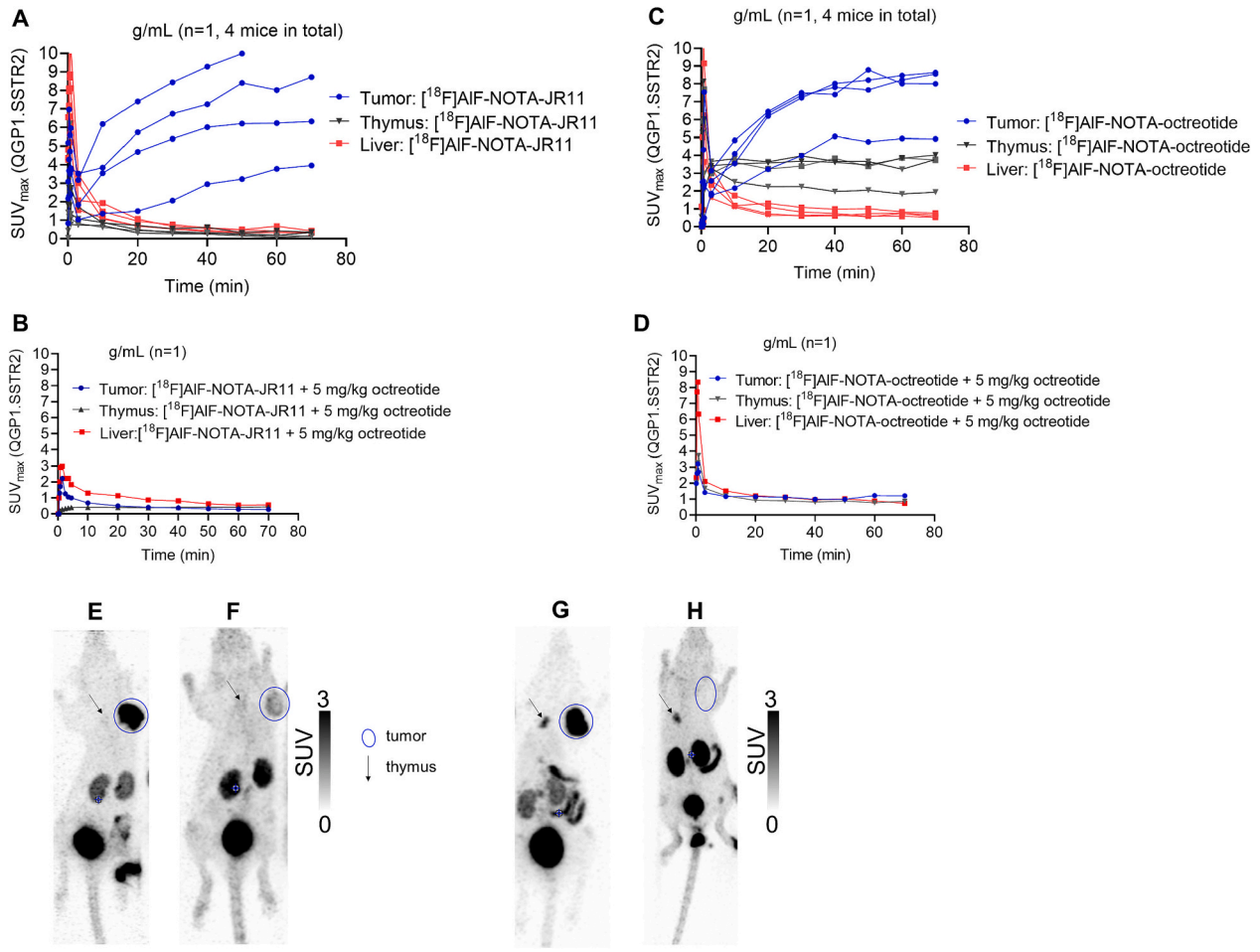

Fig. 5. TACs (SUV_{max}) representing PET/CT imaging of QGP1.SSTR2 tumor-bearing mice: (A) [^{18}F]AlF-NOTA-JR11; (B) [^{18}F]AlF-NOTA-JR11 + 5 mg/kg octreotide; (C) [^{18}F]AlF-NOTA-octreotide; (D) [^{18}F]AlF-NOTA-octreotide +5 mg/kg octreotide; MIP image (65–75 min p.i.): (E) [^{18}F]AlF-NOTA-JR11; (F) [^{18}F]AlF-NOTA-JR11 + 5 mg/kg octreotide; G) [^{18}F]AlF-NOTA-octreotide; (H) [^{18}F]AlF-NOTA-octreotide +5 mg/kg octreotide. Blue circles and black arrows indicate tumor and thymus regions respectively. (For interpretation of the references to color in this figure legend, the reader is referred to the web version of this article.)

Table 3
Preclinical comparative studies between SST antagonist (JR11) labeled tracers and SST agonist (TATE) radiotracers.

Radiotracer	Uptake	Tumor type
[^{68}Ga]Ga-DOTA-JR11[a]	23.8 ± 3.7%IA/g	HEK-hSSTR2 tumor mice [12]
[^{68}Ga]Ga-NODAGA-JR11[a]	30.7 ± 1.6 %IA/g	
[^{68}Ga]Ga-DOTA-TATE[b]	17.8 ± 2.2 %IA/g	
[^{64}Cu]Cu-NODAGA-JR11[a]	7.7 ± 2.5%IA/g	HEK-hSSTR2 tumor mice [32]
[^{64}Cu]Cu-DOTA-TATE[b]	2.8 ± 0.23%IA/g	
[^{18}F]AlF-NOTA-JR11[a]	9.02 ± 0.92 %IA/g	HEK293-SSTR2 tumor mice
[^{68}Ga]Ga-DOTA-TATE[b]	31.35 ± 5.9 %IA/g	[18]

[a] Antagonist.
[b] Agonist.

uptake of JR11 labeled tracers in both animal and human studies. Table 3 is a summary of preclinical studies comparing *in vivo* tumor binding affinity of SST antagonist (JR11) labeled tracers with SST agonist (TATE) radiotracers. It seems that not only the agonistic and antagonistic properties are important for optimal tumor accumulation, but also the tumor type, radionuclide and chelator might influence the tumor uptake.

Krebs et al. conducted the first-in-humans research of [^{68}Ga]Ga-DOTA-JR11, which revealed rapid tumor and high tumor-to-background ratios [14]. In addition, Nicolas et al. directly compared the sensitivity of [^{68}Ga]Ga-NODAGA-JR11 and [^{68}Ga]Ga-DOTA-TOC and demonstrated that the antagonist outperformed the agonist in terms of sensitivity, lesion detection, and image contrast in humans [30]. However, Zhu et al. recorded overall lower primary tumor uptake of [^{68}Ga]Ga-DOTA-JR11 than [^{68}Ga]Ga-DOTA-TATE (SUV_{max}: 18.7 ± 17.4 *vs* 32.1 ± 23.7 respectively; $p = 0.013$) in NET patients [31]. A similar trend was observed in other organs including the liver (SUV_{max}: 18.6 ± 12.5 *vs* 27.3 ± 15.4 for [^{68}Ga]Ga-DOTA-JR11 and [^{68}Ga]Ga-DOTA-TATE respectively; $p < 0.001$).

Differences in SSTR affinity may explain the variability in these reported results. The SSTR2 affinity of [^{68}Ga]Ga-NODAGA-JR11 is comparable to that of [^{68}Ga]Ga-DOTA-TOC (IC_{50}: 1.2 *vs.* 2.5 nmol/L) but substantially higher than that of [^{68}Ga]Ga-DOTA-JR11 (IC_{50}: 29 nmol/L) [31]. Similarly, [^{177}Lu]Lu-DOTA-JR11 exhibits a substantially higher affinity for SSTR2 than [^{68}Ga]Ga-DOTA-JR11 (IC_{50} = 0.73 *vs* 29 nmol/L) [31]. Also, *in vitro* experiments to determine the SSTR2 affinity of JR11 in the (HEK-hSSTR2 cell line) demonstrated the effect of using different non-radioactive metals and chelators [8]. Yttrium- or indium-DOTA complex (IC_{50}: 0.47 ± 0.05 *versus* 3.8 ± 0.7) retained a high SSTR2 affinity comparable to the DOTA-JR11 (IC_{50}: 0.72 ± 0.12). Copper and especially gallium displayed the lowest SSTR2 affinity (IC_{50}: 16.0 ± 1.2 *versus* 29.0 ± 2.7). Interestingly, when DOTA was replaced by NODAGA, the effect of gallium on SSTR2 affinity was totally restored (IC_{50}: 1.2 ± 0.2) [12].

In terms of cell binding, [^{18}F]AlF-NOTA-JR11 outperformed [^{18}F]AlF-NOTA-octreotide. However, in an *in vivo* setting, both tracers

demonstrated comparable and specific uptake in both BON-1.SSTR2 and QGP-1.SSTR2 xenografts, though uptake in QGP-1.SSTR2 was generally higher. The reason for the comparable tumor uptake of both tracers despite higher *in vitro* binding of [^{18}F]AlF-NOTA-JR11 might be the 11-fold lower affinity of [^{nat}F]AlF-NOTA-JR11 compared to [^{nat}F]AlF-NOTA-octreotide for SSTR2. Novel Al^{18}F-labeled JR11 derivatives with higher affinity might result in higher *in vivo* tumor accumulation as described for other high affinity JR11 derivatives [12,18,32].

Also, the improved imaging properties of [^{18}F]AlF-NOTA-JR11 compared to [^{68}Ga]Ga-DOTA-TATE observed by Xie et al. in the human studies could be attributed to lower liver background observed for JR11 rather than higher tumor uptake. In a clinical setting, we also observed lower liver background for [^{18}F]AlF-NOTA-octreotide compared to [^{68}Ga]Ga-DOTA-TATE, resulting in increased tissue-to-background ratio [3].

4. Conclusion

[^{18}F]AlF-NOTA-JR11 was synthesized in good RCY with RCP of 94 %. [^{18}F]AlF-NOTA-JR11 demonstrated superior *in vitro* cell binding in comparison to [^{18}F]AlF-NOTA-octreotide. However, [^{nat}F]AlF-NOTA-octreotide demonstrated 11-fold lower IC_{50} values over [^{nat}F]AlF-NOTA-JR11. Both radiotracers displayed similar *in vivo* tumor uptake with rapid renal clearance and limited bone uptake indicating excellent *in vivo* stability. [^{18}F]AlF-NOTA-octreotide showed consistent and sustained thymus uptake whereas [^{18}F]AlF-NOTA-JR11 demonstrated lower thymus uptake, indicating different affinities of both compounds for different subtypes of SSTRs. Although *in vitro* studies were very encouraging, *in vivo* studies did not show improved tumor targeting of [^{18}F]AlF-NOTA-JR11 compared to [^{18}F]AlF-NOTA-octreotide in our SSTR2 overexpressing tumor models. Novel high affinity Al^{18}F-labeled JR11 derivatives might be valuable tools to increase NET imaging sensitivity. Further, toxicity of therapeutic JR11 derivatives needs to be evaluated carefully as the compound might also be binding to low SSTR expressing, non-cancerous, tissue due to increased binding potential.

Ethics statement

The animal study was reviewed and approved by Ethical Committee for Animal Experimentation, KU Leuven.

CRediT authorship contribution statement

Experimental design, execution and data analysis was performed by Stephen Ahenkorah, Frederik Cleeren, Christopher Cawthorne and Erika Murce. Writing – original draft preparation, Stephen Ahenkorah, Christopher Cawthorne and Frederik Cleeren; writing – review and editing, Stephen Ahenkorah, Frederik Cleeren, Christopher Cawthorne, Maarten Ooms, Thomas Cardinaels, Erika Murce, Yann Seimbille, Guy Bormans and Christophe M. Deroose. All authors contributed to the article and approved the submitted version.

Funding

SCK CEN Academy support is gratefully acknowledged. This research was funded by the Education and Research Foundation for Nuclear Medicine and Molecular imaging and Neuroendocrine Tumor Research Foundation (Nuclear Medicine Pilot research grant in Neuroendocrine Tumors, F. Cleeren) and by internal funding KU Leuven. Christophe M. Deroose is a Senior Clinical Investigator at the FWO. Christopher Cawthorne was funded by FWO I000321N as well as the Department of Imaging and Pathology at KU Leuven.

Declaration of competing interest

The authors have declared that no competing interest exists.

Acknowledgements

The authors thank Julie Cornelis from the Laboratory for Radiopharmaceutical research for her contributions and Dr. Janke Kleynhans for her graphical abstract design.

References

[1] Strosberg J, El-Haddad G, Wolin E, Hendifar A, Yao J, Chasen EM B, Kunz PL, Kulke MH, Jacene H, Bushnell D, O'Dorisio RPB TM, Kulkarni HR, Caplin M, Lebtahi R, Hobday T, Delpassand EVC E, Benson A, Srirajaskanthan R, Pavel M, Mora J, Berlin J, Grande NR E, Seregni E, Öberg K, Sierra MLopera, Santoro P, Thevenet JLE T, Ruszniewski P, Kwekkeboom D, E. Krenning for the N-1 TI. Phase 3 trial of 177Lu-dotatate for midgut neuroendocrine tumors. N Engl J Med 2017;2 (376). 135–35.

[2] Deroose CM, Hindié E, Kebebew E, Goichot B, Pacak K, Taïeb D, et al. Molecular imaging of gastroenteropancreatic neuroendocrine tumors: current status and future directions. J Nucl Med 2016;57(12):1949–56.

[3] Pauwels E, Cleeren F, Tshibangu T, Koole M, Serdons K, Dekervel J, et al. [18F]AlF-NOTA-octreotide PET imaging: biodistribution, dosimetry and first comparison with [68Ga]Ga-DOTATATE in neuroendocrine tumour patients. Eur J Nucl Med Mol Imaging 2020;47(13):3033–46.

[4] Pauwels E, Cleeren F, Tshibangu T, Koole M, Serdons K, Boeckxstaens L, et al. 18F-AlF-NOTA-octreotide outperforms 68Ga-DOTA-TATE/-NOC PET in neuroendocrine tumor patients: results from a prospective, multicenter study. J Nucl Med 2022;63(10). jnumed.122.264563.

[5] Laverman P, D'Souza CA, Eek A, McBride WJ, Sharkey RM, Oyen WJG, et al. Optimized labeling of NOTA-conjugated octreotide with F-18. Tumour Biol 2012; 33(2):427.

[6] Ahenkorah S, Murce E, Cawthorne C, Ketchemen JP, Deroose CM, Cardinaels T, et al. 3p-C-NETA: a versatile and effective chelator for development of Al18F-labeled and therapeutic radiopharmaceuticals. Theranostics 2022;12(13):5971–85.

[7] Pauwels E, Cleeren F, Bormans G, Deroose CM. Somatostatin receptor PET ligands - the next generation for clinical practice. Am J Nucl Med Mol Imaging 2018;8(5): 311.

[8] Ginj M, Zhang H, Waser B, Cescato R, Wild D, Wang X, et al. Radiolabeled somatostatin receptor antagonists are preferable to agonists for in vivo peptide receptor targeting of tumors. Proc Natl Acad Sci U S A 2006;103(44):16436–41.

[9] Cescato R, Waser B, Fani M, Reubi JC. Evaluation of 177Lu-DOTA-sst2 antagonist versus 177Lu-DOTA-sst2 agonist binding in human cancers in vitro. J Nucl Med 2011;52(12):1886–90.

[10] Wadas TJ, Eiblmaier M, Zheleznyak A, Sherman CD, Ferdani R, Liang K, et al. Preparation and biological evaluation of 64Cu-CB-TE2A-sst2-ANT, a somatostatin antagonist for PET imaging of somatostatin receptor-positive tumors. J Nucl Med 2008;49(11):1819–27.

[11] Fani M, Nicolas GP, Wild D. Somatostatin receptor antagonists for imaging and therapy. J Nucl Med 2017;58:61S–6S.

[12] Fani M, Braun F, Waser B, Beetschen K, Cescato R, Erchegyi J, et al. Unexpected sensitivity of sst2 antagonists to N-terminal radiometal modifications. J Nucl Med 2012;53(9):1481–9.

[13] Albrecht J, Exner S, Grötzinger C, Prasad S, Konietschke F, Beindorff N, et al. Multimodal imaging of 2-cycle PRRT with 177Lu-DOTA-JR11 and 177Lu-DOTA-TOC in an orthotopic neuroendocrine xenograft tumor mouse model. J Nucl Med 2021;62(3):393–8.

[14] Krebs S, O'Donoghue JA, Biegel E, Beattie BJ, Reidy D, Lyashchenko SK, et al. Comparison of 68Ga-DOTA-JR11 PET/CT with dosimetric 177Lu-satoreotide tetraxetan (177Lu-DOTA-JR11) SPECT/CT in patients with metastatic neuroendocrine tumors undergoing peptide receptor radionuclide therapy. Eur J Nucl Med Mol Imaging 2020;47(13):3047–57.

[15] Reidy-Lagunes D, Pandit-Taskar N, O'Donoghue JA, Krebs S, Staton KD, Lyashchenko SK, et al. Phase I trial of well-differentiated neuroendocrine tumors (NETs) with radiolabeled somatostatin antagonist 177Lu-satoreotide tetraxetan. Clin Cancer Res 2019;25(23):6939–47.

[16] Lin Z, Lin R, Zhang J, Yao S, Miao W. 68Ga-DOTATATE and 68Ga-NODAGA-JR11 PET/CT images in a patient with gastric neuroendocrine tumor. Clin Nucl Med 2021;46(10):853–5.

[17] Wild D, Fani M, Fischer R, Del Pozzo L, Kaul F, Krebs S, et al. Comparison of somatostatin receptor agonist and antagonist for peptide receptor radionuclide therapy: a pilot study. Nucl Med 2014;55(8):1248–52.

[18] Xie Q, Liu T, Ding J, Zhou N, Meng X, Zhu H, et al. Synthesis, preclinical evaluation, and a pilot clinical imaging study of [18F]AlF-NOTA-JR11 for neuroendocrine neoplasms compared with [68Ga]Ga-DOTA-TATE. Eur J Nucl Med Mol Imaging 2021;48(10):3129–40.

[19] Dude I, Zhang Z, Rousseau J, Hundal-Jabal N, Colpo N, Merkens H, et al. Evaluation of agonist and antagonist radioligands for somatostatin receptor imaging of breast cancer using positron emission tomography. EJNMMI Radiopharm Chem 2017;2(1).

[20] Tshibangu T, Cawthorne C, Serdons K, Pauwels E, Gsell W, Bormans G, et al. Automated GMP compliant production of [18F]AlF-NOTA-octreotide. EJNMMI Radiopharm Chem 2020;5(1):4.

[21] Ory D, Van den Brande J, de Groot T, Serdons K, Bex M, Declercq L, et al. Retention of [18F]fluoride on reversed phase HPLC columns. J Pharm Biomed 2015;111: 209–14.

[22] Exner S, Prasad V, Wiedenmann B, Grötzinger C. Octreotide does not inhibit proliferation in five neuroendocrine tumor cell lines. Front Endocrinol 2018;9 (APR).
[23] Fridman R, Benton G, Aranoutova I, Kleinman HK, Bonfil RD. Increased initiation and growth of tumor cell lines, cancer stem cells and biopsy material in mice using basement membrane matrix protein (Cultrex or Matrigel) co-injection. Nat Protoc 2012;7(6):1138–44.
[24] Reubi JC, Schär JC, Waser B, Wenger S, Heppeler A, Schmitt JS, et al. Affinity profiles for human somatostatin receptor subtypes SST1-SST5 of somatostatin radiotracers selected for scintigraphic and radiotherapeutic use. Eur J Nucl Med 2000;27(3):273–82.
[25] Tircso G, Webber BC, Kucera BE, Young VG, Woods M. Analysis of the conformational behavior and stability of the SAP and TSAP isomers of lanthanide (III) NB-DOTA-type chelates. Inorg Chem 2011;50(17):7966–79.
[26] Dalm SU, Nonnekens J, Doeswijk GN, De Blois E, DiC Van Gent, Konijnenberg MW, et al. Comparison of the therapeutic response to treatment with a 177Lu-labeled somatostatin receptor agonist and antagonist in preclinical models. J Nucl Med 2016;57(2):260–5.
[27] Reubi JC, Waser B, Mäcke H, Rivier J. Highly increased 125I-JR11 antagonist binding in vitro reveals novel indications for sst2 targeting in human cancers. J Nucl Med 2017;58(2):300–6.
[28] Kübler E, Albrecht H. Large set data mining reveals overexpressed GPCRs in prostate and breast cancer: potential for active targeting with engineered anti-cancer nanomedicines. Oncotarget 2018;9(38):24882.
[29] Ten bokum AMC, Rosmalen JGM, Hofland LJ, Krenning EP, Van hagen PM, Breeman WAP. Tissue distribution of octreotide binding receptors in normal mice and strains prone to autoimmunity. Nucl Med Commun 2002;23(10):1009–17.
[30] Nicolas GP, Schreiter N, Kaul F, Uiters J, Bouterfa H, Kaufmann J, et al. Sensitivity comparison of 68Ga-OPS202 and 68Ga-DOTATOC PET/CT in patients with gastroenteropancreatic neuroendocrine tumors: a prospective phase II imaging study. J Nucl Med 2018;59(6):915–21.
[31] Zhu W, Cheng Y, Wang X, Yao S, Bai C, Zhao H, et al. Head-to-head comparison of 68Ga-DOTA-JR11 and 68Ga-DOTATATE PET/CT in patients with metastatic, well-differentiated neuroendocrine tumors: a prospective study. J Nucl Med 2020;61(6): 897–903.
[32] Rylova SN, Stoykow C, Del Pozzo L, Abiraj K, Tamma ML, Kiefer Y, et al. The somatostatin receptor 2 antagonist 64Cu-NODAGA-JR11 outperforms 64Cu-DOTA-TATE in a mouse xenograft model. PLoS One 2018;13(4).